Planning of Solar Photovoltaics, Battery Energy Storage System and Gas Micro Turbine for Coupled Micro Energy Grids

Jing Qiu
The Commonwealth Scientific and Industrial Research Organization (CSIRO), Energy Center, Mayfield West, NSW 2304, Australia, qiujing0322@gmail.com
Junhua Zhao
Chinese University of Hong Kong, Shenzhen, Guangdong, 518172, China, Junhua.zhao@outlook.com
Hongming Yang
School of Electrical and Information Engineering, Changsha University of Science and Technology, Changsha 410114, China, yhm5218@hotmail.com
Dongxiao Wang
Center for Intelligent Electricity Networks, University of Newcastle, Callaghan, NSW2308, Australia, dong.wang@uon.edu.au
Zhao Yang Dong,
School of Electrical Engineering and Telecommunications, University of New South Wales, Sydney, NSW 2052, Australia
zydong@ieee.org

ABSTRACT: This paper presents the planning of solar photovoltaics (PV), battery energy storage system (BESS) and gas-fired micro turbine (MT) in a coupled micro gas and electricity grid. The proposed model is formulated as a two-stage stochastic optimization problem, including the optimal investment in the first stage and the optimal operation in the second stage. To better understand the mutual interactions between electric and heat energy, the gas network models are taken into account. As a result, the fuel availability and price of the gas-fired MT can be explicitly modeled and analyzed. Moreover, to enhance the computational efficiency of the formulated mixed-integer quadratic programming problem, the point estimation method is used as the scenario reduction technique. The effectiveness of the proposed model is verified on a 14-bus coupled micro energy grid. Based on the case studies, the proposed two-stage planning model can identify a planning solution with the objective value of $99.3104, which is comprised of the daily capital recovery cost of $20.5070, the daily operating cost of $78.8034 for the coupled micro gas and electricity grid. Comparative studies demonstrate that the proposed approach can help the microgrid operator identify feasible and optimal planning solutions, and provide valuable guidance for energy infrastructure expansion from an integrated perspective.

Keywords: Coupled Microgrid, Coordinated System Planning, Controllable Load, Natural Gas Systems

1. Introduction

Although the paradigm of microgrids is originally targeted at electricity grids, this concept can be extended to a variety of small-scale energy loads, energy storage devices, and energy supply resources. To support the integration of renewable energy, the microgrid faces considerable investments to install BESS and MT [1]. In a case that a microgrid cannot completely rely on re-

newable energy, the natural gas grid still plays a critical role in providing power and heat to the local area[2], [3]. Hence an electrical microgrid becomes the form of coupled micro energy grids[4], [5]. A gas-fired MT is the bridge that couples micro gas and electricity grids at the supply side; while dual fuel energy devices increase the interconnection of the energy grids at the demand side [2]. Therefore, it is of great significance to address the problem of sizing, sitting of solar PV, BESS and gas-fired MT, and investigate the mutual operational impacts of the two grids from an integrated perspective [2].

In the literature, optimization models have been widely applied to other fields such as precipitation analysis and irrigation management [6], [7], [8], [9], [10]. On the other hand, the planning of BESS or distributed generation (DG) (renewable or thermal DG) in the energy system planning field can be classified to two categories: 1) optimal sizing [11], [12]; 2) optimal allocation (sitting and sizing decision) [13], [14]. Meanwhile, depending on whether DG and BESS are simultaneously considered in decision-making, the optimal planning can be classified into optimal allocation of storage or DG [15], [16] and coordinated optimal allocation [17], [18]. Some of the references are briefly described here. Ref. [3] presents a mixed-integer linear programming model for the optimal sizing, placement and operation of a multi-energy microgrid. The electrical power flow and heat transfer equations have been included, and hence the physical and operational constraints of electrical and heating/cooling networks can be modeled. Unfortunately, ref. [3] fails to model the thermal/cooling energy flows explicitly, and only energy balance constraints are included. In the meantime, models of energy storage devices such as BESS and gas linepack are completely excluded. Ref. [4] presents the optimal allocation of combined heat and power (CHP)-based DG, by introducing an integrated system dispatch model, including electricity, water, natural gas network models. The model can effectively investigate the mutual interactions between different networks. However, the model in [4] fails to investigate the role of controllable load (CL) and energy storage in terms of smoothing renewable energy and enhancing system efficiency. Ref. [19] presents a tri-objective design of an off-grid PV/wind/split-diesel/battery hybrid energy system, aiming to minimize the lifecycle cost, emissions and dump energy. The genetic algorithm is used to solve the formulated non-linear optimization problem. The proposed approach can achieve reductions in fuel consumption, emissions and replacement costs. However, the sizing of BESS is based on the battery autonomous days, so the discharge or charge efficiencies have been neglected. Ref. [20] presents the allocation of DG for radial distribution networks. The formulated objective is to minimize the network power loss and the maximum node voltage deviation. The adaptive genetic algorithm is applied to solve the formulated problem. Ref. [21] presents an interval optimization method for the optimal sizing of BESS in a hybrid PV/diesel/ESS ship power system. Also, the impact of ship swinging has been modeled based on a series of experiments, and the interval uncertainty of PV is characterized on a moving ship. Ref. [22] proposes a two-stage stochastic programming for day-ahead unit commitment and dispatch decision, in combination with a Markov decision process at a daily timescale. After obtaining the Markov decision process, the future operating costs can be predicted and the optimal sizing of wind farm and BESS can be determined based on a surrogate function optimization. To relax the equality constraint of energy balances, the general daily demand profile has been characterized by two peaks. As a result, the hourly BESS operating profile cannot be modeled. Ref. [23] proposes the DG allocation for minimizing energy loss and enhancing voltage stability based on benefit-cost analysis. Efforts have been made to propose an optimal power factor, which can be used to calculate the active and reac-

tive power sizes required by DG. Ref. [24] proposes a chance-constrained stochastic optimization model for the optimal location and capacity of BESS, aiming to maximize wind power utilization and minimize the investment and operation costs. Ref. [25] presents the optimal location and capacity of DG units, in order to minimize the system losses. The DG active power, power factor, and location are jointly considered. However, most of the above-mentioned references have not taken into account the fuel supplies for thermal DG units. In other words, the fuel price and availability of thermal DG/MT units are totally based on assumptions. Moreover, the demand response (DR) programs such as controllable load are also not well addressed in those models. Ref. [26] presents the optimal sizing of hybrid wind, PV, diesel generation for a stand-alone power system. The Markov models are employed for the system load, wind turbines and PV. The objective is to minimize the installation and unit cost as well as fuel cost, and the optimization problem is solved by the GA algorithm. Ref. [27] presents a dynamic two-stage model for the integrated allocation of wind and PV DG units, gas-fired DG units, and smart metering, as well as network reinforcement simultaneously. A nodal-based DR model is employed to capture the responsiveness to real-time pricing. The formulated objective is to minimize the total economic and carbon-emission costs. In the studies above, the fuel of thermal units is normally assumed to be unlimited and the fuel cost variation of DG is excluded.

To sum up, three main research gaps are found in the existing literature, as follows. 1) Most of the proposed models in the literature use linear programming and only consider the energy balance constraints, thereby neglecting some important parameters of network constraints (e.g. reactive power and gas pressure). 2) The demand conversion between thermal and electric energy is not well addressed. 3) The interacting operations of electricity and natural gas networks are not modelled (e.g. the fuel prices and requirements of gas-fired micro turbines are based on assumptions). To address these research gaps, this paper proposes a two-stage stochastic optimal allocation of BESS, as well as PV and gas-fired DG units integrally. Given the intermittency of solar energy, models of hot water system (HWS) and interruptible load (IL) are explicitly considered to analyse their roles in smoothing and storing solar energy. The two-stage optimization problem is comprised of the first stage *here-and-now* allocation decisions and the second stage *wait-and-see* operation decisions for the coupled gas and electricity microgrids. The gas and electricity market timeline mismatch is taken into account, and the arbitrage benefits of energy storage (such as gas linepack and BESS) are analyzed. Furthermore, the proposed model can effectively investigate the mutual interactions of gas and electricity on the microgrid operational performance. The integrated investment and operation decisions can be made to provide valuable guidance for microgrid planning.

2. Problem Description

As seen in Fig. 1, this paper assumes that a microgrid operator jointly plans and operates a coupled micro electricity and natural gas grid. This operator aims to minimize the energy procurement cost in the electricity and natural gas pool markets, by investing and efficiently utilizing the distributed energy resources (DERs) in the microgrid, such as MT, fuel cell (FC), solar PV, IL and BESS. The electricity spot market structure is on a 5-min basis, while gas pool market is on a 4-h basis during daytime and on an 8-h basis during night time. The microgrid is a price-taker in markets. More detailed information about this joint Australian gas and electricity pool market structure can be found in [28]. Moreover, in the microgrid the load aggregator performs as an

agent to represent end-users to participate in system operations. It is assumed that the load aggregator is authorized to directly manage, monitor and control the HWS and IL units of end users.

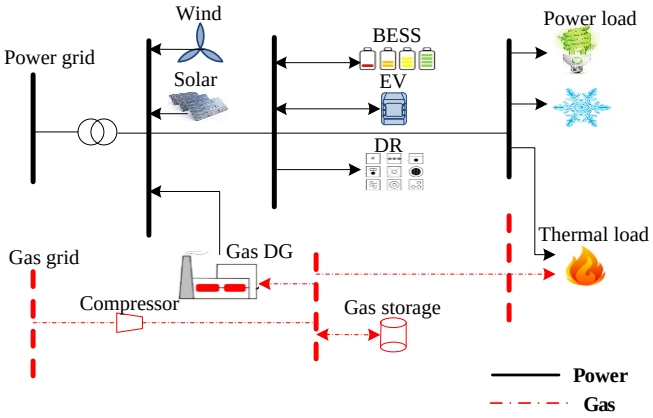

Fig. 1. A coupled micro electricity and natural gas grid.

3. Mathematical Formulation

This section introduces the detailed mathematical models used in this paper, including gas network model, solar PV model, fuel cell cost model, and controllable load model.

3.1 Gas Network Model

1) Linepack model

Linepack is the pressurized gas stored in pipelines throughout the gas networks. Linepack is proportional to the average pressure in a pipe [29]. Gas in pipes can be described by four variables, i.e., gas pressure p (kPa), volume H (m^3), density $\hbar$ (kg/m^3) and temperature Γ^{Gas} (K). According to the *Boyle's law*, gas variables are expressed as [30]:

$$\frac{p_0}{\hbar_0 \Gamma_0} = \frac{p}{\hbar \Gamma^{Gas}} = \Theta \tag{1}$$

$$p^{Aver} H_{ij} = p_0 H_0 \tag{2}$$

where p_0, H_0, $\hbar_0$, Γ_0 are gas pressure, volume, density and temperature under normal conditions; Θ is a constant. In a pipe, gas volume is equal to the pipe volume capacity. The steady state average pressure in a gas pipe can be expressed as $p_{ij}^{Aver} = \sqrt{1/2\left(p_i^2 + p_j^2\right)}$. In a steady state, the initial LP measured in energy (GJ) ($\Pi_{ij}^{Initial}$) under normal conditions is [30]:

$$\Pi_{ij}^{Initial} = \Lambda \cdot p_{ij}^{Aver} \cdot H_{ij} / \hbar_0 \cdot \Gamma_0 \cdot \Theta \tag{3}$$

where Λ denotes the constant that coverts gas volume under the normal condition to energy (GJ/m^3).

In dynamic situations, based on the *law of conservation of mass*, LP changes with the initial gas stored in pipes, the net difference between the supplied and consumed gas in a pipe[29]. Dynamic LP $\Pi_{ij,t+1}$ is described as follows.

$$\Pi_{ij,t+1} = \Pi_{ij,t} + P_{ij,t}^{Gas} \Delta t \tag{4}$$

$$P_{ij,t}^{Gas} = P_{Gijt}^{Gas} - P_{Dijt}^{Gas} - P_{ijt}^{Gas,Comp} \tag{5}$$

$$\underline{\Pi}_{ij,t} \le \Pi_{ij,t} \le \overline{\Pi}_{ij,t} \tag{6}$$

where P_{Gijt}^{Gas}, P_{Dijt}^{Gas}, $P_{ijt}^{Gas,Comp}$ denote supplied gas, gas demands, gas consumed by compressors between $i-j$; Δt denotes a factor that converts power (GJ/h) to energy (GJ), i.e., time duration; $\underline{(\bullet)}, \overline{(\bullet)}$ denote lower and upper bounds respectively.

2) Flow equation

Gas flows in a steady state can be modeled by the *Weymouth's formula*. Gas flows S_{ij}^{gas} and directions sgn_{ij} are dependent on nodal pressure differences, given as [29]:

$$S_{ij}^{gas} = sgn(p_i, p_j) \cdot \Phi_{ij} \cdot \sqrt{\left| p_i^2 - p_j^2 \right|} \tag{7}$$

$$sgn(p_i, p_j) = \begin{cases} 1; & if \ p_i \ge p_j \\ -1; & if \ p_i < p_j \end{cases} \tag{8}$$

where Φ_{ij} is a gas pipeline constant in relation to diameter, length, temperature, altitude, roughness etc.; p_i, p_j is the pressure at nodes i or j.

3) Compressor station equation

The energy consumed by a gas compressor (GC) depends on the amount of gas flows, and the difference between outlet and inlet gas pressures, as shown in empirical equations below [29].

$$S_{ij}^{Gas,Comp} = sgn(p_i, p_j) \cdot \frac{HP_{ij}}{\gamma_{1,ij} - \gamma_{2,ij} \cdot \left[\frac{max(p_i, p_j)}{min(p_i, p_j)} \right]^{\gamma_{3,ij}}} \tag{9}$$

$$P_i^{Gas,Comp}(HP_{ij}) = a_{3,ij}^{Comp} + a_{2,ij}^{Comp} \cdot HP_{ij} + a_{1,ij}^{Comp} \cdot HP_{ij}^2 \tag{10}$$

where $S_{ij}^{Gas,Comp}$ denotes gas flow in compressor between $i-j$; HP_{ij} denotes horse power for gas compressors; $\gamma_{1,ij}$, $\gamma_{2,ij}$, $\gamma_{3,ij}$ denotes coefficients for the compressor between $i-j$; $a_{1,ij}^{Comp}$, $a_{2,ij}^{Comp}$, $a_{3,ij}^{Comp}$ are horse power coefficients of the gas compressor; $P_i^{gas,Comp}$ is the gas consumption of the compressor (GJ/h). Moreover, the compressor pressure ratio CPR_{ij}^{Comp} is also bounded as:

$$\underline{CPR}_{ij}^{Comp} \le \frac{max(p_i, p_j)}{min(p_i, p_j)} \le \overline{CPR}_{ij}^{Comp} \tag{11}$$

3.2 Solar PV Model

The solar PV power output is assumed to follow a linear function of the solar radiation as [31]:

$$P_{ti}^{PV}\left(I_{ti}\right)=\eta_{PV}\cdot AS_i\cdot I_{ti}\cdot\left(1-0.005\left(t_0-25\right)\right) \tag{12}$$

where η_{PV} is the conversion efficiency; AS_i is the array size (m^2); P_{ti}^{PV}, I_{ti} are solar output and radiation (kW/m^2) at time t bus i; t_0 denotes the ambient temperature.

3.3 Fuel Cell (FC) Cost Model

FC units use an electrochemical process to turn hydrogen and oxygen into pollution free electricity and heat. The cost of FC can be presented by [12]:

$$C_{ti}^{Cell}\left(P_{ti}^{Cell}\right)=\alpha_{1i}P_{ti}^{Cell} \tag{13}$$

$$0\le P_{ti}^{Cell}\le\overline{P}_{ti}^{Cell} \tag{14}$$

where C_{ti}^{Cell}, P_{ti}^{Cell} denote the cost and power output of FC at time t and bus i; α_{1i} is cost coefficient of FC.

3.4 Controllable Load (CL) Model

In this paper, the HWS and interruptible heating ventilation air-conditioning (HVAC) loads are considered as CL. Specifically, the HWS plays a role of energy storage but without operation or life-cycle degradation cost. Meanwhile, the HVAC load is IL that is coordinated and controlled by the local agent (aggregator). Incentives are paid to customers who reduce (positive IL) or increase (negative IL) their HVAC energy consumption when requested.

1) Hot water system (HWS) model

We assume that the water volume in the HWS is constant. In other words, HWS is refilled simultaneously. Also, the insulation loss of HWS is assumed to follow a linear function of water temperature, and the temperature of inlet water (Γ_0) is assumed to be 20°C. The HWS can be modelled:

$$E_{ti}^{HWS}=E_{t-1,i}^{HWS}+\chi_{ti}^{HWS}\eta^{HWS}\overline{P}_i^{HWS}\Delta t-E_{Dti}^{HWS}-E_{ti}^{Loss} \tag{15}$$

$$E_{ti}^{HWS}=\frac{\left(\Gamma_{ti}^{HWS}-\Gamma_0\right)\cdot\Psi\cdot V_i}{3600} \tag{16}$$

$$\underline{\Gamma}^{HWS}\le\Gamma_{ti}^{HWS}\le\overline{\Gamma}^{HWS} \tag{17}$$

$$E_{ti}^{Loss}=\varpi\cdot\left(\Gamma_{ti}^{HWS}-\Gamma_0\right)=\varpi\cdot\frac{3600\cdot E_{ti}^{HWS}}{\Psi\cdot V_i} \tag{18}$$

$$E_{0i}^{HWS}=E_{i,Initial}^{HWS};E_{Ti}^{HWS}\ge E_{i,End}^{HWS} \tag{19}$$

where χ_{ti}^{HWS} is the binary variable denoting the ON/OFF status of HWS; Δt is a time factor con-

verting power (kW) to energy (kWh); η^{HWS} denote HWS charge efficiency; Γ_{ti}^{HWS} is the water temperature at time t and bus i; Ψ denotes the specific heat of water (4.186 kJ/kg^{o}C); V_i is the water volume of HWS; E_{Dti}^{HWS} is the energy demand of HWS (kWh) at time t and bus i, which is converted from the hot water volume and temperature by (16); ϖ the heat loss factor (kWh/^{o}C); E_{ti}^{Loss} is the energy loss of HWS. The energy stored in HWS at time t and bus i ,i.e., E_{ti}^{HWS}, is expressed as the net sum of energy stored at time $t-1$, the charged energy, consumed energy and the energy loss at time t, as given in (15) and (16). We assume that end-users can only control the ON/OFF status of HWS, and the charge power is not a variable. The water temperature is bounded by (17); the energy loss is calculated by (18); and (19) states the constraints on the initial ($E_{i,Initial}^{HWS}$) and the final energy ($E_{i,End}^{HWS}$) stored in HWS.

2) Cost of interruptible heating ventilation air-conditioning (HVAC) load model

We assume that load aggregators can directly control (increase or decrease) HVAC loads. Incentives paid to customers can be modelled by a quadratic cost function as below[32]:

$$C_{ti}^{IL} = \frac{1}{2}\ell_1 (P_{ti}^{IL})^2 + \ell_2 P_{ti}^{IL}, \forall i \in \Omega_D \tag{20}$$

$$\underline{\phi}_{ti} P_{Dti} \le P_{ti}^{IL} \le \bar{\phi}_{ti} P_{Dti} \tag{21}$$

where C_{ti}^{IL}, P_{ti}^{IL} denote cost and adjusted power of interruptible HVAC load; ℓ_1, ℓ_2 denote cost coefficients of IL; $\underline{\phi}_{ti}$, $\bar{\phi}_{ti}$ denote lower and upper bounds of IL; P_{Dti} denotes power demand at time t and bus i; Ω_D denotes the set of load buses.

4. Proposed Two-stage Stochastic Model

The optimal sitting and sizing of MT, PV and BESS and the optimal operation of the coupled micro energy grids are realized at two coordinated timescales. The planning problem is formulated into a two-stage stochastic programming model. In the first stage *here-and-now* allocation decisions are made before the actual realization of the uncertain data at the operational level. In the second stage, after a realization of uncertain data becomes available, a *wait-and-see* decision is made to compensate for a possible inconsistency between the prediction and reality in the first stage. The objective of the two-stage stochastic programming problem is given:

$$\text{Min} \quad g(\boldsymbol{\beta}) + O \tag{22}$$

where $\boldsymbol{\beta}$ denotes the vector of optimal sitting and sizing decisions of MT, PV and BESS; O denotes the expected operation cost. The first terms in (22) are calculated using (23).

$$g(\boldsymbol{\beta})=\sum_{i\in\Omega_N}\begin{pmatrix}\beta_i^{BESS}\cdot CF^{BESS}\cdot E_R^{BESS}+\beta_i^{MT}\cdot CF^{MT}\cdot\overline{P}_{Gi}\\+\beta_i^{PV}\cdot CF^{PV}\cdot\overline{P}_i^{PV}\end{pmatrix} \tag{23}$$

where β_i^{BESS}, β_i^{MT}, β_i^{PV} are integer decision variables denoting how many BESS, MT and PV should be built at bus i; CF^{BESS}, CF^{G}, CF^{PV} are capital recovery factors on a daily basis[1]; E_R^{BESS}, $\overline{P}_{Gi}$, $\overline{P}_i^{PV}$ are rated energy capacity of BESS and maximum active power outputs of MT and PV respectively; Ω_N denotes the set of all buses.

4.1 Detailed Models of the Second-stage

In the second stage, the objective is to minimize the sum of costs of MT, IL, BESS, FC, power exchanged and gas purchased, as given:

$$O=\mathrm{E}\begin{bmatrix}f_1(P_{Gti})+f_2(P_{ti}^{IL})+f_3(P_{ti}^{BESS})+f_4(P_{ti}^{Cell})\\+f_5(P_t^{Ex})+f_6(P_{Gt}^{Gas})\end{bmatrix} \tag{24}$$

where P_{Gti}, P_{ti}^{IL}, P_{ti}^{BESS}, P_{ti}^{Cell} denote active power outputs of MT, IL, BESS, FC at time t and bus i; P_t^{Ex} P_{Gt}^{Gas} denote the exchanged power and purchased gas at time t.

Each term in (24) is calculated as:

$$\begin{cases}f_1(P_{Gti})=\sum_{i\in\Omega_N}\sum_{t\in T}\left[a_{1i}P_{Gti}^2+a_{2i}P_{Gti}\right]\\a_{1i}=CVF_1\cdot z_t^{Gas};a_{2i}=CVF_2\cdot z_t^{Gas}\end{cases} \tag{25}$$

$$f_2(P_{ti}^{IL})=\sum_{i\in\Omega_D}\sum_{t\in T}\left[\frac{1}{2}\ell_1(P_{ti}^{IL})^2+\ell_2P_{ti}^{IL}\right] \tag{26}$$

$$f_3(P_{ti}^{BESS})=\sum_{i\in\Omega_N}\sum_{t\in T}\left[\phi^{BESS}\cdot P_{ti}^{DBESS}+\phi^{BESS}\cdot P_{ti}^{CBESS}\right] \tag{27}$$

$$f_4(P_{ti}^{Cell})=\sum_{i\in\Omega_{FC}}\sum_{t\in T}\left[\alpha_{1i}P_{ti}^{Cell}\right] \tag{28}$$

$$f_5(P_t^{Ex})=f_5(P_t^{Imp},P_t^{Exp})=\sum_{t\in T}z_t^{Imp}\cdot P_t^{Imp}-\sum_{t\in T}z_t^{Exp}P_t^{Exp} \tag{29}$$

$$f_6(P_{Gt}^{Gas})=\sum_{t\in T}z_t^{Gas}\cdot P_{Gt}^{Gas} \tag{30}$$

where a_{1i}, a_{2i} denote generation cost coefficients of MT; CVF_1, CVF_2 denote cost conversion factors , i.e., converting gas price ($/GJ) to generation cost coefficients; z_t^{Gas} is the gas price; P_{ti}^{DBESS}, P_{ti}^{CBESS} are non-negative dis/charged power of BESS, which are introduced to eliminate the nonlinearity of BESS power profile; ϕ^{BESS} is the cost coefficient of BESS, which is dependent

on life-cycles and investment cost of BESS; $P_t^{\mathrm{Im}p}$ denotes the purchased power at price z_t^{Imp}; P_t^{Exp} denotes the sold power at price z_t^{Exp}; Ω_{FC} denotes the set of FC; T denotes total time horizon.

4.2 Constraints

1) Power nodal balance

$$\begin{pmatrix} P_{Dti} + P_{ti}^{CBESS} - P_{ti}^{IL} \\ -P_{Dti}^{Curt} + P_t^{Exp} \end{pmatrix} = \begin{pmatrix} P_{Gti} + P_{ti}^{PV} + P_{ti}^{DBESS} \\ -\chi_{ti}^{HWS}\overline{P}_i^{HWS} + P_{ti}^{Cell} + P_t^{Imp} \end{pmatrix} \tag{31}$$

where P_{Dti}^{Curt} denotes the curtailed power.

2) Gas nodal balance

$$P_{Gti}^{Gas} + P_{ti}^{DLP} + \sum S_{tij}^{Gas} = \sum S_{tji}^{Gas} + P_{Dti}^{Gas} + P_{ti}^{CLP} + P_{ti}^{Gas,Comp} \tag{32}$$

$$P_{Dti}^{Gas} = P_{Dti}^{Gas,MT} + P_{Dti}^{Gas,Heat} \tag{33}$$

where P_{ti}^{DLP}, P_{ti}^{CLP} denote discharged and charged linepack respectively; $P_{Dti}^{Gas,MT}$, $P_{Dti}^{Gas,Heat}$ denote gas demand for MT and non-electric gas demand respectively; S_{tij}^{Gas} denote gas flow between $i-j$ at time t.

3) Linepack constraint

$$\Pi_{ij,t+1} = \Pi_{ij,t} + P_{ti}^{CLP}\Delta t - P_{ti}^{DLP}\Delta t + P_{tj}^{CLP}\Delta t - P_{tj}^{DLP}\Delta t \tag{34}$$

$$\underline{\Pi}_{ij,t} \le \Pi_{ij,t} \le \overline{\Pi}_{ij,t} \tag{35}$$

$$0 \le P_{ti}^{CLP} \le \chi_{ti}^{CLP} \cdot DF \tag{36}$$

$$0 \le P_{ti}^{DLP} \le \chi_{ti}^{DLP} \cdot DF \tag{37}$$

$$\chi_{ti}^{CLP} + \chi_{ti}^{DLP} \le 1 \tag{38}$$

where DF denotes the disjunctive factor (a very large positive value); χ_{ti}^{CLP}, χ_{ti}^{DLP} are binary variables denoting the charge and discharge decisions of linepack, and they cannot be 1 at the same time.

4) Power flow constraint

$$PL_{tij} - \gamma_{ij}\left(\theta_{ti} - \theta_{tj}\right) = 0 \tag{39}$$

$$\underline{PL}_{ij} \le PL_{tij} \le \overline{PL}_{ij} \tag{40}$$

where PL_{tij}, γ_{ij} denote active power flow and susceptance; θ_{ti}, θ_{tj} denote voltage angles.

5) Gas flow constraint

Gas network constraints (7)-(11) are linearized by the first-order Taylor series approximation proposed in [33].

6) MT and PV generation constraints

$$\beta_i^{MT} \cdot \underline{P}_{Gi} \le P_{Gti} \le \beta_i^{MT} \cdot \overline{P}_{Gi}\,; \forall i \in \Omega_N \tag{41}$$

$$\beta_i^{MT} \cdot \overline{P}_{Gti} \le P_{Dti}^{Gas,MT} \cdot HR^{Gas} \cdot \Delta t \tag{42}$$

$$\begin{cases} P_{Gti} - P_{Gt-1,i} \le \beta_i^{MT} \cdot RU_{Gi} \\ P_{Gt-1,i} - P_{Gti} \le \beta_i^{MT} \cdot RD_{Gi} \end{cases}; \forall i, j \in \Omega_N \tag{43}$$

$$0 \le P_{ti}^{PV} \le \beta_i^{PV} \overline{P}_i^{PV}\,; \forall i \in \Omega_N \tag{44}$$

where RU_{Gi}, RD_{Gi} denote ramping up and ramping down limits of MT at bus i; HR^{Gas} is the heat rate of gas (kW/GJ) considering the energy efficiency of MT. Equation (42) states that the output of MT is subject to the gas availability. Note that constraints (41)-(42) can be easily extended to CHP units with simple modification. This is not in the scope of this paper [33].

7) BESS constraints

$$E_{t+1,i}^{BESS} = E_{t,i}^{BESS} - \Delta t P_{ti}^{DBESS} / \eta_D + P_{ti}^{CBESS} \eta_C \Delta t \tag{45}$$

$$\beta_i^{BESS} \cdot E_R^{BESS} \cdot \underline{SOC} \le E_{ti}^{BESS} \le \beta_i^{BESS} \cdot E_R^{BESS} \cdot \overline{SOC} \tag{46}$$

$$0 \le P_{ti}^{DBESS} \le \beta_i^{BESS} \overline{P}^{DBESS} \tag{47}$$

$$0 \le P_{ti}^{CBESS} \le \beta_i^{BESS} \overline{P}^{CBESS} \tag{48}$$

$$E_{0i}^{BESS} = \beta_i^{BESS} \cdot E_{i,Initial}^{BESS}; E_{Ti}^{BESS} \ge \beta_i^{BESS} \cdot E_{i,End}^{BESS} \tag{49}$$

where $E_{t,i}^{BESS}, SOC_{ti}$ denote the energy stored in BESS and state-of-charge (SOC) at time t and bus i; η_D, η_C denote discharge and charge efficiency; (47)-(48) are introduced to remove the nonlinearities of the BESS power profile. Equation (49) defines the initial and final energy in BESS. Be noted that binary variables for dis/charge decisions are not needed, provided that the BESS dis/charge efficiencies are different.

8) System reserve constraints

$$\begin{cases} \sum_{i\in\Omega_N} \beta_i^{MT} \overline{P}_{Gi} + \sum_{i\in\Omega_{GS}} \beta_i^{PV} \overline{P}_i^{PV} + \overline{P}^{Ex} \ge \sum_{i\in\Omega_D} (1+RU) P_{Dti} \\ \sum_{i\in\Omega_N} \beta_i^{MT} \underline{P}_{Gi} - \overline{P}^{Ex} \le \sum_{i\in\Omega_D} (1-RD) P_{Dti} \end{cases} \tag{50}$$

where RU, RD denote system ramping up and ramping down reserve.

9) Fuel cell constraints

FC constraints include (13) and (14).

10) Controllable load constraints

CL constraints include (15)-(21).

11) Interconnection constraints

$$\begin{cases} 0 \le P_t^{Imp} \le \chi_t^{Imp} \overline{P}^{Ex} \\ 0 \le P_t^{Exp} \le \chi_t^{Exp} \overline{P}^{Ex} \end{cases} \tag{51}$$

$$\chi_t^{Imp} + \chi_t^{Exp} \le 1 \tag{52}$$

where $\overline{P}_t^{Ex}$ denotes the upper bound of the exchanged power; χ_t^{Imp}, χ_t^{Exp} are binary decision variables of importing and exporting power.

12) Load curtailment and reliability constraints

$$LOLE = \sum_{i \in \Omega_D} \sum_{t \in T} P_{Dti}^{Curt} \le \overline{LOLE} \tag{53}$$

$$P_{Dti}^{Curt} \le P_{Dti}; \forall i \in \Omega_D \tag{54}$$

where $LOLE$ denotes loss of load expectation, which is a reliability measure for microgrids.

4.3 Scenario Construction and Reduction

In this paper, solar generation, load, electricity and gas prices are considered as uncertainties. The stochastic variations of the uncertainties from their predicted values are assumed to follow the Beta distribution (i.e., solar forecast errors) [34] and the normal distribution (i.e., electricity and gas prices, and load forecast errors) respectively [35]. To enhance the computational efficiency, the point estimation method is used [36].

If the operation cost vector is denoted by $\mathbf{O}$, the kth term O_k is caused by the uncertainty in the variable x_k. The nonlinear function f_k is expressed as:

$$O_k = f_k(x_1, x_2, \ldots x_k, \ldots x_m) \tag{55}$$

where x_k is a random variable. The total number of random variables is m. Each x_k is assumed to be a random variable with known mean and variance based on historical data or expert knowledge.

Note that for a $L \times m$ scheme the statistical information provided by the first few moments is concentrated on L points for each variable x_k, named *concentration.* In other words, the deterministic problem has to be solved L times for each input random variable. The lth concentration of the random variable x_k is represented by a location $x_{k,l}$ and a weight $w_{k,l}(x_{k,l}, w_{k,l})$. Also, the relation between the input and output variables is represented by a nonlinear function $F(x_1, x_2, \ldots, x_k, \ldots x_m)$ with m input random variables. The location $x_{k,l}$ is determined by:

$$x_{k,l} = \mu_{x_k} + \xi_{k,l} \sigma_{x_k} \tag{56}$$

where $\xi_{k,l}$ is the standard location, and μ_{x_k} and σ_{x_k} are the mean and standard deviation of the input random variable x_k.

The standard location $\xi_{k,l}$ and the weight $w_{k,l}$ are obtained by solving the following nonlinear equations:

$$\sum_{l=1}^{L} w_{k,l} = \frac{1}{m} \tag{57}$$

$$\sum_{l=1}^{L} w_{k,l}\left(\xi_{k,l}\right)^n = \psi_{k,n} \quad n = 1, 2, \ldots, 2L-1 \tag{58}$$

where $\psi_{k,n}$ is the nth standard central moment of the random variable x_k with probability density function f_{x_k}, and that is:

$$\psi_{k,n} = \frac{M_n\left(x_k\right)}{\left(\sigma_{x_k}\right)^n} \tag{59}$$

Note that $\psi_{k,1}$ equals zero, $\psi_{k,2}$ equals one, and $\psi_{k,3}$ and $\psi_{k,4}$ are the skewness and kurtosis of x_k. The nth central moment of the random variable x_k is

$$M_n\left(x_k\right) = \int_{-\infty}^{+\infty}\left(x_k - \mu_{x_k}\right)^n f_{x_k}\, dx_k \tag{60}$$

Once all the concentrations $\left(x_{k,l}, w_{k,l}\right)$ are obtained, the nonlinear function F is used to calculate the vector of random output variables of the operation cost $O\left(k,l\right)$ at each point $\left(\mu_{x_1}, \mu_{x_2}, \ldots, x_{k,l}, \ldots, \mu_{x_m}\right)$:

$$O\left(k,l\right) = F\left(\mu_{x_1}, \mu_{x_2}, \ldots, x_{k,l}, \ldots, \mu_{x_m}\right) \tag{61}$$

The $2m+1$ scheme can provide the desired statistical information regarding random output variables by solving (57)-(58) for $L = 3$ and $\xi_{k,3} = 0$. The standard locations and weights are:

$$\xi_{k,l} = \frac{\psi_{k,3}}{2} + \left(-1\right)^{3-l}\sqrt{\psi_{k,4} - \frac{3}{4}{\psi_{k,3}}^2} \quad l = 1, 2 \;\; \xi_{k,3} = 0 \tag{62}$$

$$w_{k,l} = \frac{\left(-1\right)^{3-l}}{\xi_{k,l}\left(\xi_{k,1} - \xi_{k,2}\right)} \quad l = 1, 2 \tag{63}$$

$$w_{k,3} = \frac{1}{m} - \frac{1}{{\psi_{k,4} - \psi_{k,3}}^2} \tag{64}$$

Note that this scheme sets $\xi_{k,3} = 0$, having $x_{k,l} = \mu_{x_k}$ in (57) and (58), and so m of the $3m$ locations are the same point $\left(\mu_{x_1}, \mu_{x_2}, \ldots, \mu_{x_k}, \ldots, \mu_{x_m}\right)$. Therefore, running one evaluation of func-

tion F at this location is enough, provided that the corresponding weight is updated to the value w_0 as follows:

$$w_0 = \sum_{k=1}^{m} w_{k,3} = 1 - \sum_{k=1}^{m} \frac{1}{\psi_{k,4} - \psi_{k,3}^{\ 2}} \tag{65}$$

By using the weighting factor $w_{k,l}$ and $O(k,l)$ values, the nth raw moments of the random output variables are estimated by:

$$E[O^n] \cong \sum_{k=1}^{m} \sum_{l=1}^{L} w_{k,l} (O(k,l))^n \tag{66}$$

Therefore, using the point estimation method, the formulated objective (22) can be rewritten as:

$$\text{Min} \quad g(\boldsymbol{\beta}) + \sum_{k=1}^{m} \sum_{l=1}^{L} w_{k,l} (O(k,l))^n \tag{67}$$

4.4 Solution Method

The formulated two-stage model is a mixed integer quadratic programming (MIQP) problem, which can be efficiently solved by commercial solvers such as CPLEX. In the first stage, the decision variables are integer variables $\beta_i^{BESS}, \beta_i^{MT}, \beta_i^{PV}$. In the second stage, the decision variables include binary variables $\chi_{ti}^{CLP}, \chi_{ti}^{DLP}, \chi_{ti}^{HWS}, \chi_t^{Imp}, \chi_t^{Exp}$ and continuous variables $P_{Gti}, P_{ti}^{DLP}, P_{Gt}^{Gas}$, P_{ti}^{CLP}, $P_{ti}^{CBESS}, P_{ti}^{DBESS}, P_{ti}^{IL}$, $P_{ti}^{Cell}, P_t^{Imp}, P_t^{Exp}, P_{Dti}^{Curt}$.

5. Case Studies

The proposed approach is tested on a coupled 14-bus gas and electricity system. The one-line diagram of the system is shown in Fig. 2 and the system data can be found in [37], [38]. The peak general load is 19.53 kW and the peak residential gas load is 0.5391 GJ/hour. The original power suppliers in the microgrid include one 5 kW solar PV, one 7 kWh BESS, one 3 kW FC, and two 5 kW MT. CL resources including HWS and HVAC are assumed to be located at all load buses and the maximum IL ratio is 10%. The water volume of HWS is 250 Liters, and the working temperature range is from 45ºC to 65ºC. The inlet water temperature is assumed to be 20ºC. The daily profiles of 5-min general load, hot water load, electricity price, residential gas demand and gas price are shown in Fig. 3 [28]. The general power load usually can be categorized into base load (e.g. load of fridges) and controllable load (e.g. load of air-conditioners or TVs). Hot water load usually refers to hot water consumption (e.g. hot water for taking a shower). Residential gas load usually refers to gas consumptions for cooking or heating. Generally speaking, the variation of the base power load is very small. However, the variations of controllable power load, hot water load and residential gas load are related to whether occupants are at home and the activities of occupants. On the other hand, the variations of electricity and gas prices are more complicated, as these variations are related to the energy market situations (e.g. the overall energy supply and demand),

time-of-use network charges, constraints of energy networks, bidding behavior of market participants, etc. The parameters of candidates of MT, BESS and PV are given in Tables 1, 2 and 3. The simulations were completed by a PC with Intel Core i7-6600 CPU @ 2.80 GHZ with 8.00 GB RAM.

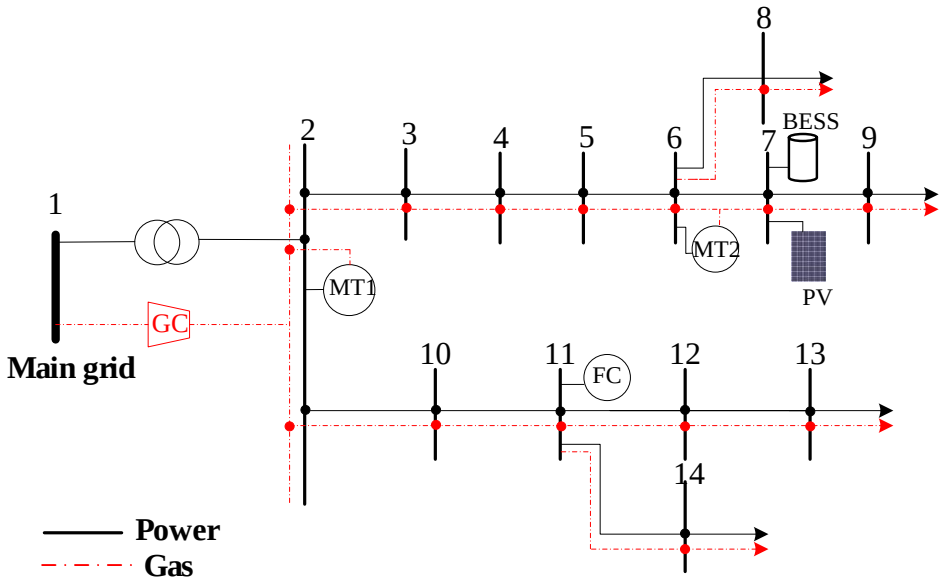

Fig. 2. One line diagram of 14-bus coupled micro energy grids.

Table 1 Parameters of candidate MT

Item	Value	Item	Value
Min. capacity	0 kW	Ramp down	0.18 kW/min
Max. capacity	2.5 kW	Investment cost	\$500/kW
Life span	20 yrs	CVF_1	0.0024
Ramp up	0.16 kW/min	CVF_2	1.0235

Table 2 Parameters of candidate BESS

Item	Value	Item	Value
Dis/charge power capacity	1.4 kW; 1.2 kW	Life cycles	3000 times
Energy capacity	2.5 kWh	Initial/ final energy	1.25 kWh
Dis/ Charge efficiency	95%; 90%	Investment cost	200 E_R^{BESS} \$

Table 3 Parameters of candidate solar PV

Item	Value	Item	Value
Max. capacity	2.5 kW	Investment cost	\$400/kW

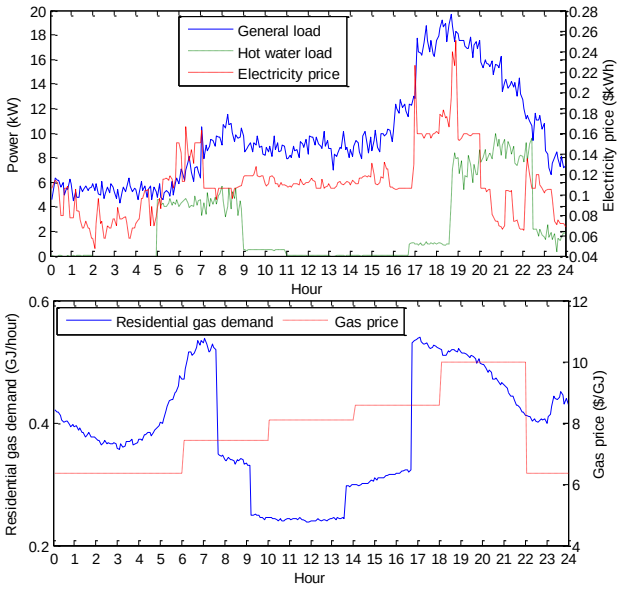

Fig. 3. Daily profiles of general load, hot water load, electricity prices, residential gas demand and gas price.

To verify the effectiveness of the proposed approach, three cases are compared: **Case 1:** A single-stage stochastic planning model for coupled micro energy grids. **Case 2:** A two-stage planning model with scenario reduction. But gas and electricity grids are operated separately. **Case 3:** The proposed two-stage planning model for the coupled micro energy grid.

Table 4 Allocation results of Case 1

Bus no./kWh/kW										
BESS (kWh)	Bus	2	3	4	5	8	10	12	13	14
	Size	12.5	10	10	10	10	10	10	10	7.5
MT (kW)	Bus	3			5			11		
	Size	10			10			5		
PV (kW)	Bus	2	3	4	5	8	10	12	13	14
	Size	5	5	5	5	5	5	5	5	5

Table 5 Allocation results of Case 2

Bus no./kWh/kW								
BESS (kWh)	Bus	2	3	4	5	6	10	11
	Size	12.5	20	15	7.5	10	15	10
MT (kW)	Bus	3			10			
	Size	15			10			
PV (kW)	Bus	2	3	4	5	6	10	11
	Size	5	10	5	5	5	10	5

The allocation results of BESS, MT and PV for cases 1-3 are given in Table 4-6. We can see that the total capacities of BESS, MT and PV for the three cases are identical, i.e., 90 kWh of BESS, 25 kW of MT, and 45 kW of PV. When gas network constraints are not considered in case

2, larger capacities of MT are located at buses 3 and 10. It should be noted that these two MT units might not be able reach their maximum capacity, since their outputs are constrained by fuel availability in the gas grid. In other words, the separated planning approach might lead to impractical operation results. Moreover, the allocation results for cases 1 and 3 are similar, except a sitting decision of MT (a 5-kW MT is sat at bus 11 for case 1 but at bus 10 for case 3).

Table 6 Allocation results of Case 3

Bus no./kWh/kW										
BESS	Bus	2	3	4	5	8	10	12	13	14
(kWh)	Size	12.5	10	10	10	10	10	10	10	7.5
MT	Bus	3			5			11		
(kW)	Size	10			10			5		
PV	Bus	2	3	4	5	8	10	12	13	14
(kW)	Size	5	5	5	5	5	5	5	5	5

Fig.4 compares the hourly exchanged power with the main grid for cases 1 and 3. Generally speaking, the microgrid prefers to sell electricity at morning and evening peaks, when the electricity price is relatively high. The PV production and electricity purchased from the grid are mainly used to charge HWS and BESS. The BESS plays a critical role in making arbitrage benefits. The total purchased electricity quantities are 39.23 kWh and 76.49 kWh for cases 1 and 3 respectively; while total sold electricity quantities are 154.68 kWh and 203.76 kWh. In contrast to the single stage planning in case 1, the proposed two-stage planning is less conservative and more energy is traded.

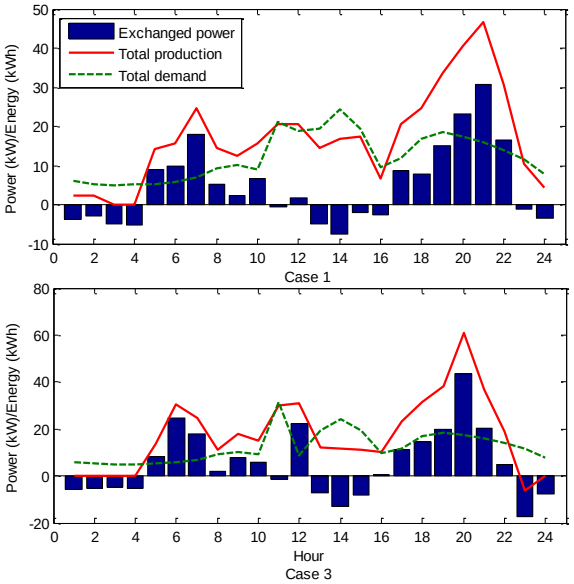

Fig. 4 Hourly exchanged power for cases 1 and 3.

The linepack variations corresponding to gas supply and demand imbalance are illustrated in Fig. 5. Since gas is dispatched at larger time intervals, the gas purchase decisions are very strategic. Compared to case 2, the coordinated gas and power grid operation buys more gas in the evening. Also, one interesting difference is that linepack is mainly consumed in the morning peak for case 2, while in the evening peak for case 3. This is because that the coordinated planning in case 3 can strategically save linepack for the MT gas demand peak in the evening. Furthermore, the

SOC of BESS corresponding to dis/charged power, outputs of MT, FC and IL is illustrated in Fig. 6. We can see that for cases 2 and 3 BESS are mainly charged between 12pm and 16 pm, and discharged in morning and evening peaks. However, for case 2, the microgrid buys electricity to charge BESS at 4 am. As a result, more BESS energy is used for the morning peak, instead of using MT, IL or FC. For case 2, the total energy amounts produced by MT, FC and IL are 201.78, 9.22 and 4.4 kWh respectively. For case 3, the total energy amounts produced by MT, FC and IL are 199.04, 8.21 and 3.91 kWh respectively. To better demonstrate the daily load of customers, in Fig. 7, we have given the 5-min power profiles at bus 7 in case 3, including BESS, HWS, solar PV, general load and net power. This customer does not have MT. BESS is discharged between 5-7 am and 17-19 pm, when the electricity prices are high. After the HWS and the BESS are charged by PV, most of the energy is exported between 10 am and 15 pm. It is worth mentioning that IL is not used, as the peak of this customer is not evident.

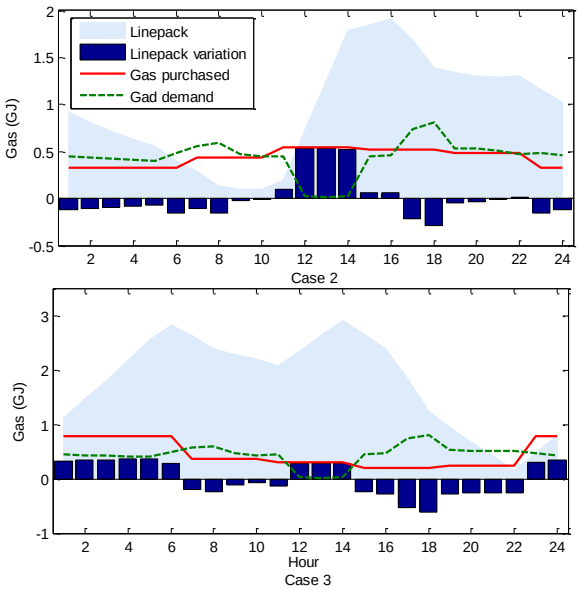

Fig. 5 Gas linepack profiles for case 2 and 3.

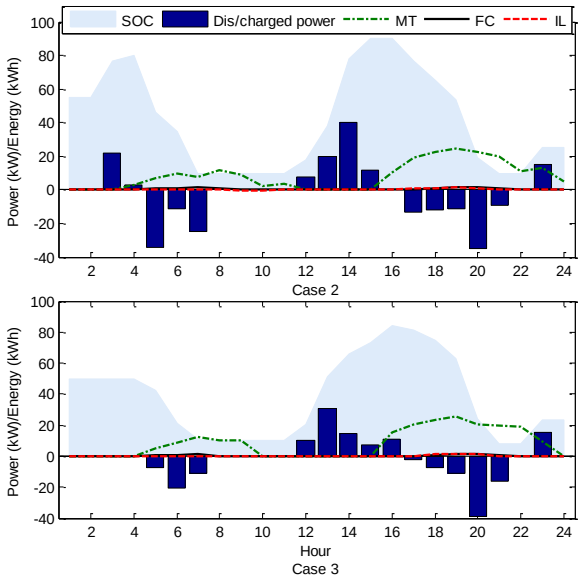

Fig. 6 SOC and outputs from MT, FC and IL for cases 2 and 3.

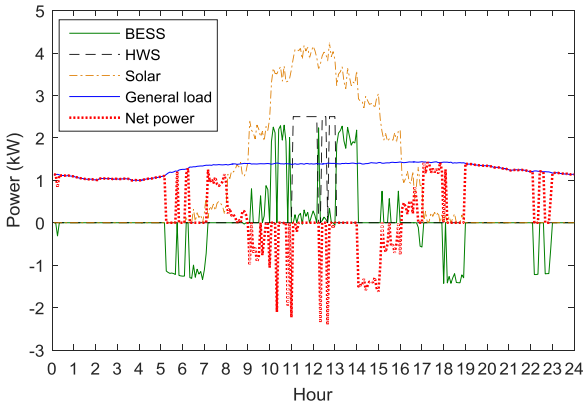

Fig. 7 Detailed 5-min power profile at bus 7 in case 3.

Table 7 compares the detailed cost compositions for cases 1-3. Although the investment cost (IC) for all cases are the same, the total operation cost (OC) is the lowest for case 3 ($78.8034). The separated planning approach in case 2 leads to inferior solutions, as the objective value is the highest ($114.6799). Moreover, case 1 is the worst in terms of the computational efficiency, as the single-stage stochastic programing approach requires 4574 seconds before it converges. Also, the single-stage planning model in case 1 fails to effectively investigate the interactions between investment and operating decisions. Compared to case 3, the total OC for case 1 is relatively higher, thus leading to a higher total cost. To sum up, the proposed approach is superior from both optimality and computational efficiency perspectives.

Table 7 Detailed result comparison for three cases

Item	**Case 1**	**Case 2**	**Case 3**
IC of BESS ($)	11.3905	11.3905	11.3905
IC of MT ($)	2.7480	2.7480	2.7480
IC of PV ($)	6.3865	6.3865	6.3865
Total IC ($)	**20.5070**	**20.5070**	**20.5070**
OC of MT ($)	7.3416	7.7892	7.2311
OC of IL ($)	0.7013	0.8865	0.6784
OC of BESS ($)	14.0622	18.9712	13.6209
OC of FC ($)	0.8236	0.8579	0.8236
Cost of power ($)	3.7062	7.6618	7.5974
Cost of gas ($)	80.9658	84.8907	76.3887
Rev. of power ($)	-19.1104	-26.8844	-27.5367
Total OC ($)	**88.4903**	**94.1729**	**78.8034**
Objective ($)	**108.9973**	**114.6799**	**99.3104**
Elapsed(seconds)	**4574**	**1012**	**986**

6. Conclusions

This paper has proposed the two-stage optimal allocation of solar PV, BESS, and gas-fired MT, including optimal sitting and sizing decisions for a coupled micro gas and electricity grid. The mutual interactions of electric and heat energy are investigated, and the optimal operation of

the microgrid aims to minimize the sum of operation cost of MT, IL, BESS, FC, power and gas exchanged with the main grid. According to the simulation results, the single stage stochastic approach suffers considerable computational burden and identifies a less economical operation strategy. The separated planning approach is likely to lead to inferior or improper solutions under the gas price and availability assumptions. By contrast, the proposed approach is capable of identifying feasible and optimal investment and operation solutions from the integrated perspective, thus providing valuable guidance for microgrid planning. Based on the case studies, the proposed two-stage planning model can identify a planning solution with the objective value of $99.3104, which is comprised of the daily capital recovery cost of $20.5070, the daily operating cost of $78.8034 for the coupled micro gas and electricity grid.

Acknowledgement

The work in this paper is supported by a China Southern Power Grid Research Grant WYKJ00000027, the National Natural Science Foundation of China (Key Program 71331001, 71420107027, 91547113 and General Program 71071025, 71271033), the Science and Technology Projects of Hunan Province and Changsha City (2016WK2015, kh1601186) and the Shenzhen Municipal Science and Technology Innovation Committee International R&D project (GJHZ20160301165723718).

References

[1] Chen C, Duan S, Cai T, Liu B, Hu G. Optimal allocation and economic analysis of energy storage system in microgrids. IEEE Trans Power Electron. Oct. 2011;26:2762-73.

[2] Yang H, Xiong T, Qiu J, Qiu D, Dong ZY. Optimal operation of DES/CCHP based regional multi-energy prosumer with demand response. Applied Energy. April 2016;167:353-65.

[3] Mashayekh S, Stadler M, Cardoso G, Heleno M. A mixed integer linear programming approach for optimal DER portfolio, sizing and placement in multi-energy microgrids. Applied Energy. Feb. 2017;187:154-68.

[4] Zhang X, Karady GG, Ariaratnam ST. Optimal allocation of CHP-based distributed generation on urban energy distribution networks. IEEE Trans Sustain Energy. Jan. 2014;5:246-53.

[5] Touretzky CR, Mc Guffin DL, Ziesmer JC, Baldea M. The effect of distributed electricity generation using natural gas on the electric and natural gas grids. Applied Energy. Sep. 2016;177:500-14.

[6] Valipour M. Study of different climatic conditions to assess the role of solar radiation in reference crop evapotranspiration equations. J of Applied Water Eng. and Res. 2014;61:679-94.

[7] Valipour M. Optimization of neural networks for precipitation analysis in a humid region to detect drought and wet year alarms. Meteorological Applications. 2015;23:91-100.

[8] Valipour M. Increasing irrigation efficiency by management strategies; cutback and surge irrigation. ARPN J of Agri and Biolo Science. Jan. 2013;8:35-43.

[9] Valipour M. How much meteorological information is necessary to achieve reliable accuracy for rainfall estimations? Agriculture. 2016;6:53

[10] Yannopoulos SI, Lyberatos G, Theodossiou N, Li W, Valipour M, Tamburrino A, et al. Evolution of water lifting devices (pumps) over the centuries worldwide. Water. 2015;7:5031-60.

[11] Yang Y, Li H, Aichhorn A, Zheng J, Greenleaf M. Sizing strategy of distributed battery storage system with high penetration of photovoltaic for voltage regulation and peak load shaving. IEEE Trans Smart Grid. Mar.

2014;5:982-91.

[12] Chen SX, Gooi HB, Wang MQ. Sizing of energy storage for microgrids. IEEE Trans Smart Grid. Mar. 2012;3:142-51.

[13] Keane A, O'Malley M. Optimal allocation of embedded generation on distribution networks. IEEE Trans Power Syst. Aug. 2005;20:1640-6.

[14] Zheng Y, Dong ZY, Luo FJ, Meng K, Qiu J, Wong KP. Optimal allocation of energy storage system for risk mitigation of DISCOs with high renewable penetrations. IEEE Trans Power Syst. Jan. 2014;29:212-20.

[15] Sedghi M, Ahmadian A, Aliakbar-Golkar M. Optimal storage planning in active distribution network considering uncertainty of wind power distributed generation. IEEE Trans Power Syst. Jan. 2016;31:304-16.

[16] Wang Z, Chen B, Wang J, Kim J, Begovic MM. Robust optimization based optimal DG placement in microgrids. IEEE Trans Smart Grid. Sept. 2014;5:2173-82.

[17] Chen C, Duan S. Optimal allocation of distributed generation and energy storage system in microgrids. IET Renew Power Gener. Aug. 2014;8:581-9.

[18] Yang P, Nehorai A. Joint optimization of hybrid energy storage and generation capacity with renewable energy. IEEE Trans Smart Grid. Jul. 2014;5:1566-74.

[19] Ogunjuyigbe ASO, Ayodele TR, Akinola OA. Optimal allocation and sizing of PV/Wind/Split-diesel/Battery hybrid energy system for minimizing life cycle cost, carbon emission and dump energy of remote residential building. Applied Energy. June 2016;171:153-71.

[20] Ganguly S, Samajpati D. Distributed generation allocation on radial distribution networks under uncertainties of load and generation using genetic algorithm. IEEE Trans Sustain Energy. Jul. 2015;6:688-97.

[21] Wen S, Hong YY, Yu DC, Zhang L, Cheng P. Allocation of ESS by interval optimization method considering impact of ship swinging on hybrid PV/diesel ship power system. Applied Energy. Aug. 2016;175:158-67.

[22] Shin J, Lee JH, Realff MJ. Operational planning and optimal sizing of microgrid considering multi-scale wind uncertainty. Applied Energy. June 2017;195:616-33.

[23] Hung DQ, Mithulananthan N, Bansal RC. An optimal investment planning framework for multiple distributed generation units in industrial distribution systems. Applied Energy. Jul. 2014;124:62-72.

[24] Zhang Y, Dong ZY, Luo F, Zheng Y, Meng K, Wong KP. Optimal allocation of battery energy storage systems in distribution networks with high wind power penetration. IET Renew Power Gener. Oct. 2016;10:1105-13.

[25] Vatani M, Alkaran DS, Sanjari MJ, Gharehpetian GB. Multiple distributed generation units allocation in distribution network for loss reduction based on a combination of analytical and genetic algorithm methods. IET Gener Transm Distrib. Oct. 2016;10:66-72.

[26] Hong YY, Lian RC. Optimal sizing of hybrid wind/PV/diesel generation in a stand-alone power system using Markov-based genetic algorithm. IEEE Trans Power Del. April 2012;27:640-7.

[27] Zeng B, Zhang J, Yang X, Wang J, Dong J, Zhang Y. Integrated planning for transition to low-carbon distribution system with renewable energy generation and demand response. IEEE Trans Power Syst. May 2014;29:1153-65.

[28] Australian Energy Market Operator (AEMO) <http://www.aemo.com.au/> [accessed 15.2.17].

[29] Kabirian A, Hemmati MR. A strategic planning model for natural gas transmission networks. Energy Policy. May 2007;35:5656-70.

[30] Chaudry M, Jenkins N, Strbac G. Multi-time period combined gas and electricity network optimisation. Elec Power Syst Res. July 2008;78:1265-79.

[31] Ruey-Hsun L, Jian-Hao L. A fuzzy-optimization approach for generation scheduling with wind and solar energy systems. IEEE Trans Power Syst Nov. 2007;22:1665-74.

[32] Mashhour E, Moghaddas-Tafreshi SM. Bidding strategy of virtual power plant for participating in energy and

spinning reserve markets-part I: problem formulation. IEEE Trans Power Syst. May 2011;26:949-56.

[33] Qiu J, Yang H, Dong ZY, Zhao JH, Meng K, Luo F, et al. A linear programming approach to expansion co-planning in gas and electricity markets. IEEE Trans Power Syst. Sep. 2016;31:3594-606.

[34] Niknam T, Zare M, Aghaei J. Scenario-based multiobjective volt/var optimization for distribution networks including renewable energy sources. IEEE Trans Power Syst. 2012;27:2004-19.

[35] Li W. Risk Assessment of Power Systems: Models, Methods, and Applications. New York: IEEE Press/Wiley; 2005.

[36] Hong HP. An efficient point estimate method for probabilistic analysis. Reliab Eng Syst Saf. June 1998;59:261-7.

[37] Wu X, Wang X, Qu C. A hierarchical framework for generation scheduling of microgrids. IEEE Trans Power Deliv. Dec. 2014;29:2448-57.

[38] Basu AK, Chowdhury S, Chowdhury SP. Impact of strategic deployment of CHP-based DERs on microgrid reliability. IEEE Trans Power Del. Jul. 2010;25:1697-705.